JACS
JOURNAL OF THE AMERICAN CHEMICAL SOCIETY

Article

pubs.acs.org/JACS

Multistate Organization of Transmembrane Helical Protein Dimers Governed by the Host Membrane

Anton A. Polyansky,*[,†,‡] Pavel E. Volynsky,[‡] and Roman G. Efremov[‡,§]

[†]Department of Structural and Computational Biology, Max F. Perutz Laboratories, University of Vienna, Campus Vienna Biocenter 5, Vienna, AT-1030, Austria

[‡]M.M. Shemyakin and Yu.A. Ovchinnikov Institute of Bioorganic Chemistry, Russian Academy of Sciences, Moscow, 117997, Russia

[§]Moscow Institute of Physics and Technology (State University), Dolgoprudny, Moscow Region, 141700, Russia

Supporting Information

ABSTRACT: Association of transmembrane (TM) helices taking place in the cell membrane has an important contribution to the biological function of bitopic proteins, among which receptor tyrosine kinases represent a typical example and a potent target for medical applications. Since this process depends on a complex interplay of different factors (primary structures of TM domains and juxtamembrane regions, composition and phase of the local membrane environment, etc.), it is still far from being fully understood. Here, we present a computational modeling framework, which we have applied to systematically analyze dimerization of 18 TM helical homo- and heterodimers of different bitopic proteins, including the family of epidermal growth factor receptors (ErbBs). For this purpose, we have developed a novel surface-based modeling approach, which not only is able to predict particular conformations of TM dimers in good agreement with experiment but also provides screening of their conformational heterogeneity. Using all-atom molecular dynamics simulations of several of the predicted dimers in different model membranes, we have elucidated a putative role of the environment in selection of particular conformations. Simulation results clearly show that each particular bilayer preferentially stabilizes one of possible dimer conformations, and that the energy gain depends on the interplay between structural properties of the protein and the membrane. Moreover, the character of protein-driven perturbations of the bilayer is reflected in the contribution of a particular membrane to the free energy gain. We have found that the approximated dimerization strength for ErbBs family can be related to their oncogenic ability.

INTRODUCTION

Membrane-driven association of transmembrane (TM) α-helices represents a basis for protein folding and oligomerization. Being functionally important, this process is controlled by many factors in the cell, such as primary structure of interacting helices, lipid composition of their local environment, binding of external or internal ligands, and general physicochemical properties of the membrane. Even in the simplest case of bitopic proteins, whose TM domains consist just of a single α-helix, oligomerization can have a strong impact on the biological function (e.g., transmembrane signal transduction) as has been shown for a wide class of receptor tyrosine kinases (RTK).[1−6] It was also hypothesized that different conformations of TM domains in a dimer of RTKs might stabilize activated or nonactivated states of the receptor via the *rotation-coupled* mechanism.[7,8] Importantly, single point mutations in the TM region of RTK can modulate efficiency of dimerization and induce dramatic changes of the protein biological function, including development of oncologic diseases.[9−11] Another equally important aspect of TM helices association *in vivo* is that it takes place in the environment exhibiting high lateral heterogeneity. Such a mixture of phospholipids with different acyl-chains, polar heads, and cholesterol undergoes microphase separation resulting in the formation of membrane microdomains, which is accompanied by a reduction of the area accessible to the free diffusion due to presence of membrane proteins in high concentration.[12,13] These factors can significantly modulate structural and dynamic properties of TM helical dimers and the dimerization process in general.[14,15]

The complexities mentioned above suggest that simple model systems usually considered to understand the mechanism of association of TM helices cannot be directly extrapolated to the real cell. For instance, experimental techniques for determination of TM helical dimer spatial structures by NMR spectroscopy in detergent micelles, or more complicated membrane mimics (bicelles)[16] typically account only for one particular conformation of a dimer promoted by such environment.[17] On the one hand, this information is crucial for design of novel potent pharmaceuticals, modulating dimerization of bitopic proteins (especially, RTKs) and representing a very promising strategy for overcoming cancer resistance toward conventional therapy.[18,4] On the other hand, given limitations might close the door to the development of

Received: April 11, 2012
Published: August 13, 2012

   dx.doi.org/10.1021/ja303483k | J. Am. Chem. Soc. 2012, 134, 14390−14400

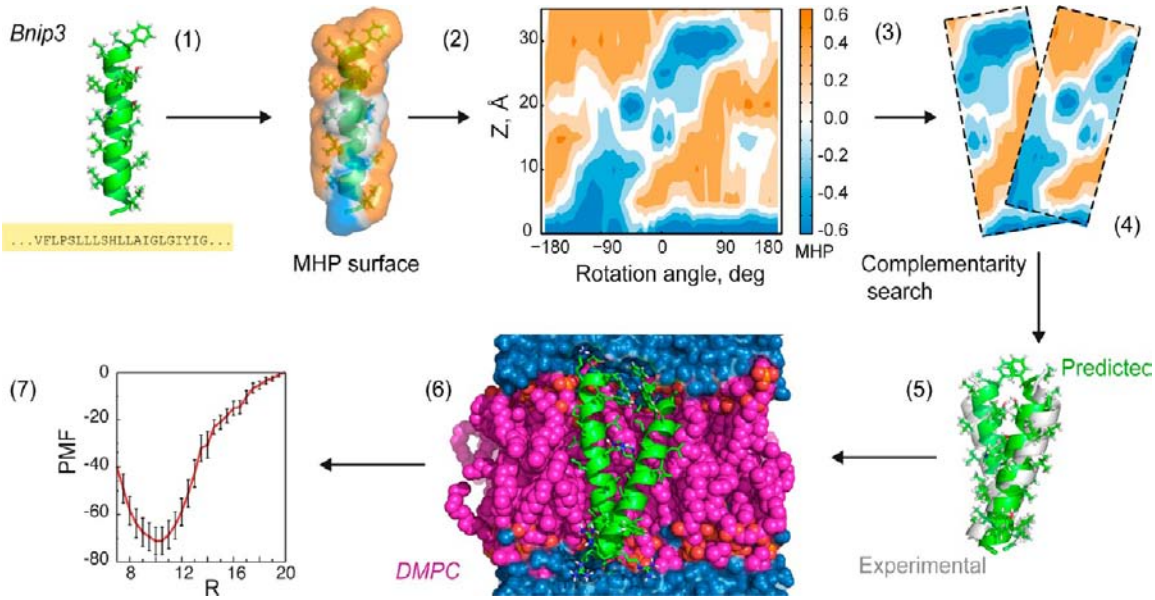

Figure 1. Modeling framework used in studies of TM helical dimers: 1 − reconstruction of TM helices from sequences; 2 − mapping of hydrophobic/hydrophilic properties on helical surfaces according to the molecular hydrophobicity potential (MHP) approach; 3 − projection of surface properties (MHP and landscape) onto the cylinder and building 2D maps (positive values of MHP correspond to hydrophobic regions); 4 − pairwise comparisons of surface fragments using a fixed widow sliding along 2D maps of respective helices, estimation of surface complementarity; 5 - reconstruction of 3D conformation of the dimer; 6 − MD relaxation of the dimer conformation in explicit bilayers; 7 − calculation of potential of mean force (PMF) profiles using umbrella sampling techniques with force integration. All steps are shown for the TM fragment of Bnip3 protein. Steps 1−5 are implemented in PREDDIMER algorithm.

Table 1. Parameters of Helical Dimers Predicted Using PREDDIMER Algorithm

dimer	sequence[a]	χ angle, deg	F_{SCOR}	L, Å	rmsd, Å
Bnip3	VFLPSLLLSHLLAIGLGIYIG	−25.2/-15.9/28.9[b]	3.3/2.7/2.7	30.6/31.1/29.4	2.0/4.2/4.9
EphA1	IVAVIFGLLLGAALLLGILVF	−51.9/-8.0/46.5	3.4/3.1/3.1	26.1/30.7/30.3	2.2/3.0/6.5
EphA2	LAVIGGVAVGVVLLLVLAGVGFFI	17.0/-29.4/62.9	3.3/3.2/3.1	34.8/33.6/32.3	1.6/5.6/6.2
ErbB1	PSIATGMVGALLLLLVVALGIGLFM	13.1/-54.3/-46.7	3.3/3.0/3.0	36.5/34.6/32.4	
ErbB1/ErbB2		−22.5/30.2/-47.6	3.8/3.8/3.6	37.7/37.2/34.9	2.4/6.3/2.2
ErbB1/ErbB3		5.5/-60.3/51.4	3.7/3.3/3.3	37.4/31.7/32.5	
ErbB1/ErbB4		13.4/47.9/-40.6	3.4/3.4/3.3	36.9/32.2/36.2	
ErbB2	PLTSIISAVVGILLVVVLGVVFGILI	28.8/-49.6/-20.0	3.5/3.4/3.1	37.6/34.8/38.0	5.6/1.6/2.6
ErbB2/ErbB3		−32.4/-52/53.7	3.5/3.5/3.5	37.2/34.8/34.3	
ErbB2/ErbB4		23.9/-22.0/60.2	3.4/3.3/3.0	38.1/37.9/33.8	
ErbB3	LTMALTVIAGLVVIFMMLGGTFLYW	−28.4/-4.2/47.0	3.5/3.1/2.9	33.9/34.5/29.3	5.8/4.6/5.0
ErbB3/ErbB4		59.7/-45.0/-60.8	3.6/3.3/3.3	33.8/34.6/31.6	
ErbB4	PLIAAGVIGGLFILVIVGLTFAVYV	−39.4/23.5/59.4	3.3/3.2/3.0	35.6/35.7/30.6	2.3/5.5/6.6
ErbB2*neu** (V664Q)	PLTSIISAV**Q**GILLVVVLGVVFGILI	51.8/-28.6/33.8	3.8/3.8/3.5	34.5/37.2/37.2	
GPA	ITLIIFGVMAGVIGTILLISYGI	−49.9/60.0/-1.0	4.3/3.7/3.7	31.0/29.8/34.3	1.6/7.3/4.0
GpAG83I	ITLIIFGVMA**I**VIGTILLISYGI	−60.6/31.2/-19.7	3.8/3.0/3.0	29.0/33.2/33.4	
GpAI76V	ITL**V**IFGVMAGVIGTILLISYGI	−43.8/-5.3/40.4	4.4/3.7/3.6	31.6/34.6/32.4	
PDGFR-β	VVVISAILALVVLTIISLIILIMLW	57.3/-43.4/4.1	3.4/3.2/3.1	32.5/35.7/37.2	4.4/5.5/2.4

[a]Sequence, TM fragment used in modeling; χ angle, crossing angle between helices; F_{SCOR}, value of the scoring function characterizing packing efficiency; L, hydrophobic length of the dimer; rmsd, root-mean-square deviation from the experimental structure; corresponding Protein Data Bank entries are 2J5D for proapototic Bnip3 protein,[30] 2K1L for Ephrin type-A receptor 1 (EphA1),[30] 2KY9 for EphA2,[8] 2KS1 for ErbB1/ErbB2 receptor tyrosine kinases heterodimer,[31] 2JWA for ErbB2,[32] 2L9U for ErbB3,[33] 2L2T for ErbB4, 1AFO for Glycophorin A (GpA),[34] 2L6W for platelet-derived growth factor receptor β (PDGFR-β).[35] [b]Values for three top predicted conformations are separated by the slash.

selective binders facilitating or blocking the dimerization, since the dimer conformations targeted in vivo are usually affected by the local membrane properties and/or lipid interactions with juxtamembrane regions.[19,15] Moreover, even estimations of the dimerization efficiency (or thermodynamics of the helix association) might vary a lot, depending on the exact technique: ToxR bacterial reporter systems (TOXCAT),[20] Förster resonance energy transfer (FRET) methods,[21] or the steric trap.[22] This often results in ambiguous conclusions about the strength of interactions of TM domains.

Finally, the prevailing conception of more than 15 years of a dimerization by-and-large driven by sequence motifs needs to be adapted in order to correspond better to recent findings in the field.[5,6] Given all this, it seems reasonable to emphasize that in general dimerization of TM helices is a problem with no single solution—one has to take into account their sequences,

dx.doi.org/10.1021/ja303483k | J. Am. Chem. Soc. 2012, 134, 14390−14400

possible conformational transitions within a dimer and in a particular lipid environment. Only a combination of all these factors can be taken to be responsible for the realistic dimer structure. In this context, computational approaches represent alternative and promising venues to complement and rationalize experimental results.[6] Nowadays, they are able to predict possible conformations of a dimer, estimate their strength of association, and analyze carefully the effects of the environment in a self-consistent way (see ref 17 for a recent review).

Here, we present a modeling framework (Figure 1) applied to systematic studies of the dimerization of nine unique TM peptides (Table 1). For some of them, we have also studied heterodimers (family of epidermal growth factor receptors (ErbBs)) and mutant analogues (glycophorin A (GpA), ErbB2). In total, we have considered 18 dimers using the same platform. We have developed a novel surface-based algorithm for the prediction of all possible dimer structures starting from sequences of the monomers and have applied it to the set of TM sequences. This was inspired by the fact that in a general case dimerization of two helices might be reduced to spatial pairwise superposition of their molecular surfaces, whose geometrical and polar characteristics encode all interaction patterns with no need to particularly consider any sequence motifs in dimer prediction.[23,24] For instance, the typical "small-xxx-small" motif is represented on the surface as a polar groove, which facilitates helices packing according to the "knob-into-hole" rule,[25] or its rephrased surface based version—*complementarity of surface landscapes*. The packing of the TM helices in the membrane environment is usually associated with the removal of polar residues from the lipid phase. This removal is accomplished by burying the polar residues in the helix−helix interface as observed in most of the experimentally obtained dimer structures.[5] Although this *"lipophobic"* effect in the membrane is not a simple inversion of the hydrophobic effect in water, it still represents entropic contribution of the environment to the dimer formation. Appearance of additional interhelical hydrogen bonds is reflected in observing *hydrophilic−hydrophilic interactions* on the dimer interface. The latter, however, in some case represents a tuning of the dimer conformation rather than the driving force of association.[26] Finally, the lipid exposed parts of the helices form the dimer surface. On average, the dimer surface becomes *smoother*, due to the packing of surface irregularities, and/or *more hydrophobic* than the surfaces of the individual monomers. The aforementioned principles of TM helix association were incorporated into the recently presented PREDDIMER algorithm intended for the prediction of TM helical dimers[17] or higher oligomers.[27]

Three dimers of distinct types (pro-apoptotic protein Bnip3, ephrin receptor EphA2, heterodimer of ErbB1 and ErbB2) have been subjected to all-atom molecular dynamics (MD) simulations in membranes composed of phosphocholine (PC) lipids with different acyl chains: $C_{14:0}C_{14:0}$PC (DMPC), $C_{16:0}C_{18:1c9}$PC (POPC), $C_{20:1c11}C_{20:1c11}$PC (DEPC). MD simulations were followed by calculation of the association free energy of the dimers in these explicit membranes differing in their physicochemical properties. Using approximately 20 μs of total MD statistics, we have shown that each particular bilayer preferentially stabilizes one of the possible conformations of a dimer, and that the energy gain depends on interplay between dimer and bilayer structural properties. Free energy decomposition into individual contributions of a protein, a bilayer, and a solvent demonstrates that, depending on the combination of a dimer and a bilayer, impact of the membrane can vary from strongly favorable to strongly unfavorable and that such different membrane behavior might depend on the character of the perturbation induced by TM peptides. Finally, to estimate relative efficiency of homo- and heterodimerization within the ErbBs family, we have established a relationship between the association free energy and packing quality of the predicted dimer. We have found that the dimerization efficiency for the family members might be related in some cases to the oncogenic activity of the respective receptors.

RESULTS AND DISCUSSION

Surface-Based Reconstruction of Helical Dimers. Starting from TM sequences, PREDDIMER algorithm performs scanning of possible superpositions of helical surfaces (or dimer conformations), estimation of their complementarity, dimer structure reconstruction followed by geometry optimization, ranking and filtering of the results. Detail steps of the procedure applied to the prediction of the dimeric structure of TM fragments of the pro-apoptotic protein Bnip3 are shown in Figure 1. First, a TM helix is built in the ideal 3D conformation and its surface hydrophobicity is mapped according to the molecular hydrophobicity potential (MHP) approach.[28] Second, the surface is projected onto the cylinder that gives MHP and landscape (α, Z) maps (where, α is the rotation angle around the helical axis and Z is the displacement along the axis). Here, one can see that the Bnip3 helix possesses a prominent hydrophilic groove, which defines its dimerization interface (Figure 1, panel 3). Third, the overlap between maps of two helices is systematically explored in 5-dimensional space ($\alpha 1$, $\alpha 2$, χ, R, d) using a sliding window procedure (see Methods). Finally, the algorithm yields several "best" (or "top") dimer structures ranked according to the values of the scoring function (F_{SCOR}). In the case of Bnip3, the first predicted conformation exhibits 2 Å backbone rmsd from the NMR structure[29] (Figure 1, panel 5, Table 1).

For each dimer reported in this study, the algorithm has considered about 10^5 of possible variants and yielded 3−7 unique dimer conformations (or cluster representatives) as a result of the prediction. Although the method described here does not operate with thermodynamic ensembles of the dimer conformations like in the case of force-field based approaches in canonical ensembles typically applied for dimer prediction,[36−39] it still has an advantage of exploration of those dimer conformations, which are not available for the latter methods due to their limited coverage of the potential energy landscape. Also, in comparison with several similar global search approaches suggested previously,[40−42] our method considers dimerization of α-helices in a more general, surface-based context without employing residual knowledge-based or force-field-like scoring functions. Importantly, PREDDIMER can be used for any molecular surface of a helical-like shape, not necessary proteins (e.g., peptido-mimetics). This makes it very promising in the design of novel drugs targeting TM protein domains.

Multistate Organization of Dimer Conformational Space. Using the described algorithm, we have predicted ensembles of possible conformations for 12 homodimers (including two GpA and one ErbB2 mutants) and 6 heterodimers of ErbB-family. Parameters of the top three (according to F_{SCOR}) distinct conformations for each dimer are given in Table 1. For the half of them, 3D structures were also obtained by NMR spectroscopy in different membrane-like

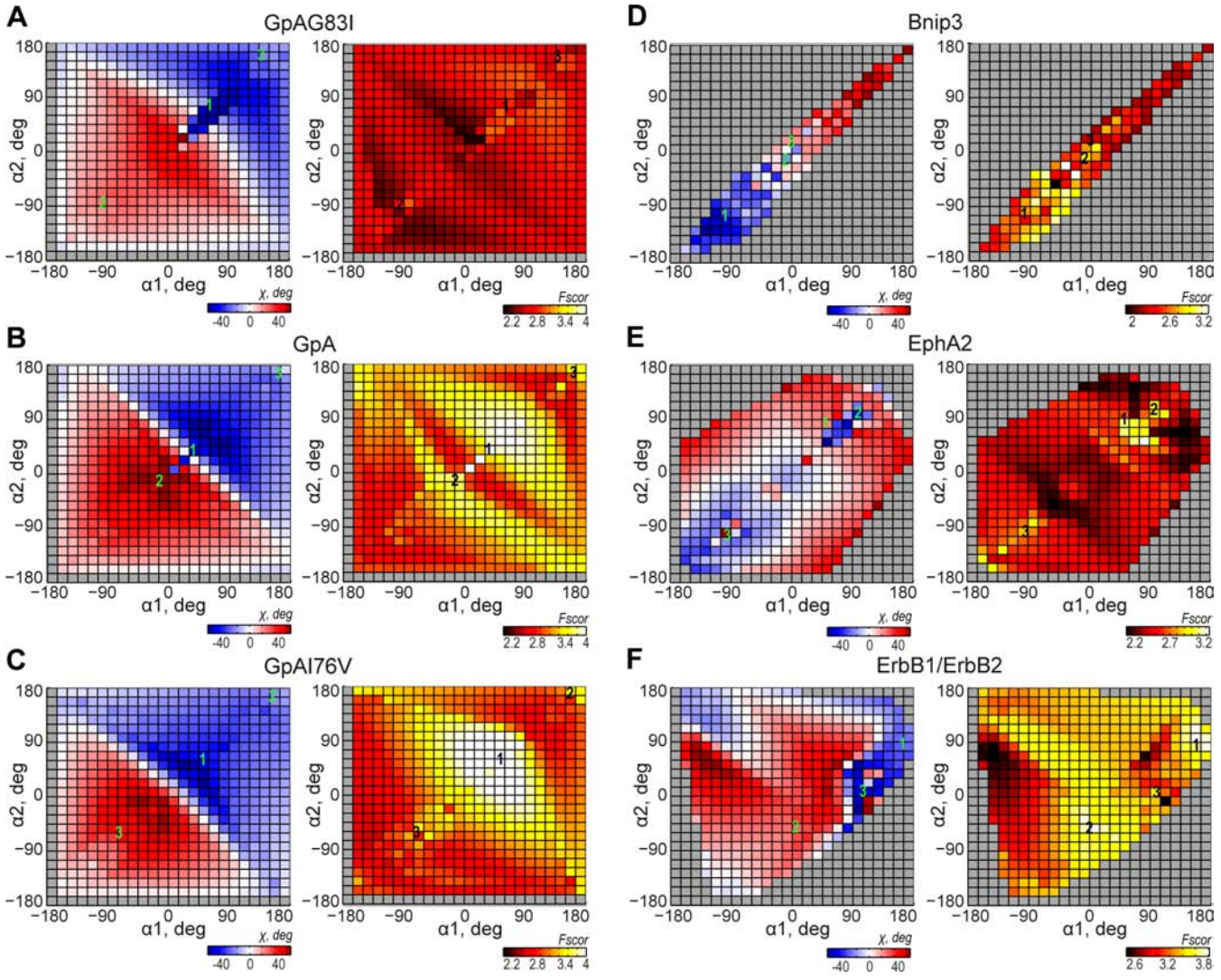

Figure 2. Heterogeneity of the conformational space for TM helical dimers: GpA and its mutants (A-C), Bnip3 (D), EphA2 (E), ErbB1/ErbB2 (F). For each dimer, 2D projections of the dimer crossing angle (χ) and the scoring function (F_{SCOR}) onto angular coordinates ($\alpha1$, $\alpha2$) are shown. High values of F_{SCOR} reflect high packing efficiency of the dimer. Maps are colored according to the scales of χ and F_{SCOR} values given below each panel. Locations of three top-scoring dimer conformations are indicated with their rank numbers. Regions where the algorithm is not able to pack helices into a dimer due to steric constrains are colored in gray.

environments. In all of those cases (except ErbB3, whose published structure has anomalous packing compared to other RTKs[33,6]), NMR-like conformation of a dimer can be found among three top solutions (usually, with the first rank) given by the algorithm. Since the latter one operates just with ideal helices, these structures exhibit backbone rmsd from respective experimental structures in the range 1.5−2.5 Å. Using ideal helices provides more "coarse-grained" initial dimer configurations, which are not located in a local minimum like in a case of any particularly optimized conformations. Further MD relaxation of the predicted models in explicit membranes usually increases their similarity to the experimental ones. For instance, after 50 ns MD simulations in a DMPC bilayer, the predicted NMR-like conformation of Bnip3 deviates by only 0.9 Å from the reference structure (Supporting Information, Table S1). Similarly, EphA2 MD dimer conformation in the DEPC bilayer exhibits 1.3 Å rmsd from the corresponding NMR model (Supporting Information, Table S1).

Here, we should emphasize that the aim of our study is not just *in silico* reconstruction of experimental-like structures, but rather exploration of different conformational possibilities for a dimer, whose structural heterogeneity can be represented by the distribution of the scoring function (F_{SCOR}) for dimer packing efficiency along three angular coordinates, ($\alpha1$, $\alpha2$, χ). Corresponding 2D projections shown in Figure 2 depict ($\alpha1$, $\alpha2$) regions colored by χ and effective F_{SCOR}, where the algorithm is able to pack helices into a dimer. As one can notice from the figure, amino-acid sequences of the helices strongly predefine "ideal" conformational space available to the dimer. This is true even for single-point G83I and I76V mutations of GpA, given here as the well-known example. Thus, G83I universally decreases packing ability of GpA (Figure 2A), while I76V causes just a small redistribution between possible right- and left-handed conformations making the latter one less favorable (Figure 2C) as compared to the wild-type dimer (Figure 2B). Moreover, the best conformations of GpAI76V and GpA (NMR-like model 1) have similar crossing χ-angles (Table 1) and locate in similar ($\alpha1$, $\alpha2$) regions suggesting almost the same interface. This agrees well with the experimental evidence of a strong destabilizing effect of the

dx.doi.org/10.1021/ja303483k | J. Am. Chem. Soc. 2012, 134, 14390−14400

G83I substitution[22,43] and just mild perturbation of the I76V one.[43] TM helices of other studied proteins represent an even more intriguing example. In the case of Bnip3, only a very narrow conformational region is available for packing (Figure 2D), and three top conformations already occupy all favorable subspaces. In contrast, more dimer variants become possible for EphA2 (Figure 2E). Interestingly, its two highest scoring structures lie in a close proximity to each other in the coordinate space ($\alpha 1$, $\alpha 2$), but have positive (left-handed, NMR-like) and negative (right-handed) values of the angle χ. We speculate that, in such a situation, the dimer might be able to switch relatively easily between the two conformations in response to the local environment (see below). Similar conformational transitions between right and left-handed dimers have already been suggested for ErbB2[7] and discussed also for EphA2[8] as a putative rotation-coupled mechanism of the activation. However, in both cases no strong experimental evidence supporting this point of view have been provided so far. The conformational space available for ErbB1/ErbB2 heterodimer is asymmetric, thus indicating limited accessibility of different sides of the monomeric helices to dimerization (Figure 2F). At the same time, many of the dimer conformations are still available making the conformational space less confined as compared to the previous cases. We speculate that such an organization makes the ErbB1/ErbB2 dimer relatively flexible allowing facile transitions between neighboring states without the need to surmount high energy barriers. Although the scoring function allows good distinction between different conformations of the same dimer, it is not applicable when comparing very different proteins because of its empirical and rather relative character (see Methods). However, based solely on the conformational heterogeneity of considered TM dimers, we suggest that their stability most likely would decrease as follows: Bnip3 > EphA2 > ErbB1/ErbB2.

Altogether, according to our prediction results, solutions for most of the dimers contain several different and equally well-packed (in terms of F_{SCOR}, Table 1) conformations including NMR-like ones. We speculate that the conformations alternative to the NMR-like ones might be realized in environments, which are different from those used in the particular experiments. More specifically, the final dimer structure is never constant, but rather represents an interplay between the peptide sequence and characteristics of the environment (see also ref 5).

Effect of the Environment on Stability of Various Dimer Conformations. To test whether it is possible that the membrane of a particular composition preferentially selects (or stabilizes) one dimer conformation over other possibilities, the predicted TM helical dimers have been subjected to MD simulations in explicit lipid bilayers. For this purpose, we have selected three illustrative examples: a dimer with the confined conformational space (Bnip3), a dimer with several equally possible conformations (EphA2), and a heterodimer with a number of possible states (ErbB1/ErbB2, see above). We have estimated the free energy of association of these models in bilayers composed of phosphocholine lipids with different acyl chains: DMPC, POPC, and DEPC. This was done using umbrella sampling techniques with the mean force integration.[44,45] Dimerization free energies for the respective 27 systems are reported in Figure 3 (full PMF profiles are shown in Supporting Information, Figure S1). According to these results, the dimers display different stability. On average, ΔG increases gradually as Bnip3 ≪ EphA2 < ErbB1/ErbB2. This corresponds well to organization of their conformational spaces (see above), and also reflects the strong dimerization nature of the Bnip3 homodimer.[29,46] Furthermore, we have found that the POPC bilayer provides systematically stronger association of TM helices as compared to DMPC or DEPC (Figure 3A). Recently, the dramatic increase of the GpA dimer stability in the POPC bilayer with respect to detergents has been estimated to be approximately 50 kJ mol^{-1}.[22] Also, in coarse-grained simulations it was shown that the dimerization of GpA is

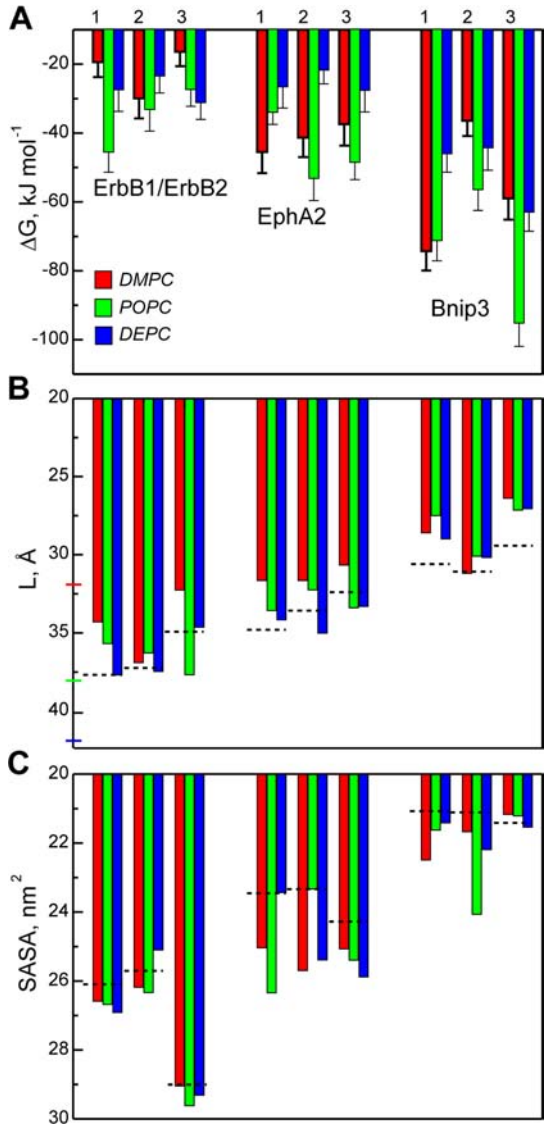

Figure 3. Relaxation of ErbB1/ErbB2, EphA2 and Bnip3 dimer conformations (three top-scoring) in different membrane media. (A) Association free energies obtained from PMF profiles (Supporting Information, Figure S1) and averaged over three independent calculations. Hydrophobic length (L, (B)) and solvent accessible surface area (SASA, (C)) of relaxed dimeric structures used in free energy calculations. Dashed lines correspond to the respective values for "ideal" nonrelaxed conformations. Parameters of each dimer model in DMPC, POPC, and DEPC bilayers are shown with red, green, and blue bars, respectively. The thickness of unperturbed bilayers (see details in the text) is indicated with additional ticks at the vertical axis in panel B using the same color code as for the bars. According to their ranks, these top-scoring models for each dimer are indicated with symbols "1", "2", and "3".

dx.doi.org/10.1021/ja303483k | J. Am. Chem. Soc. 2012, 134, 14390−14400

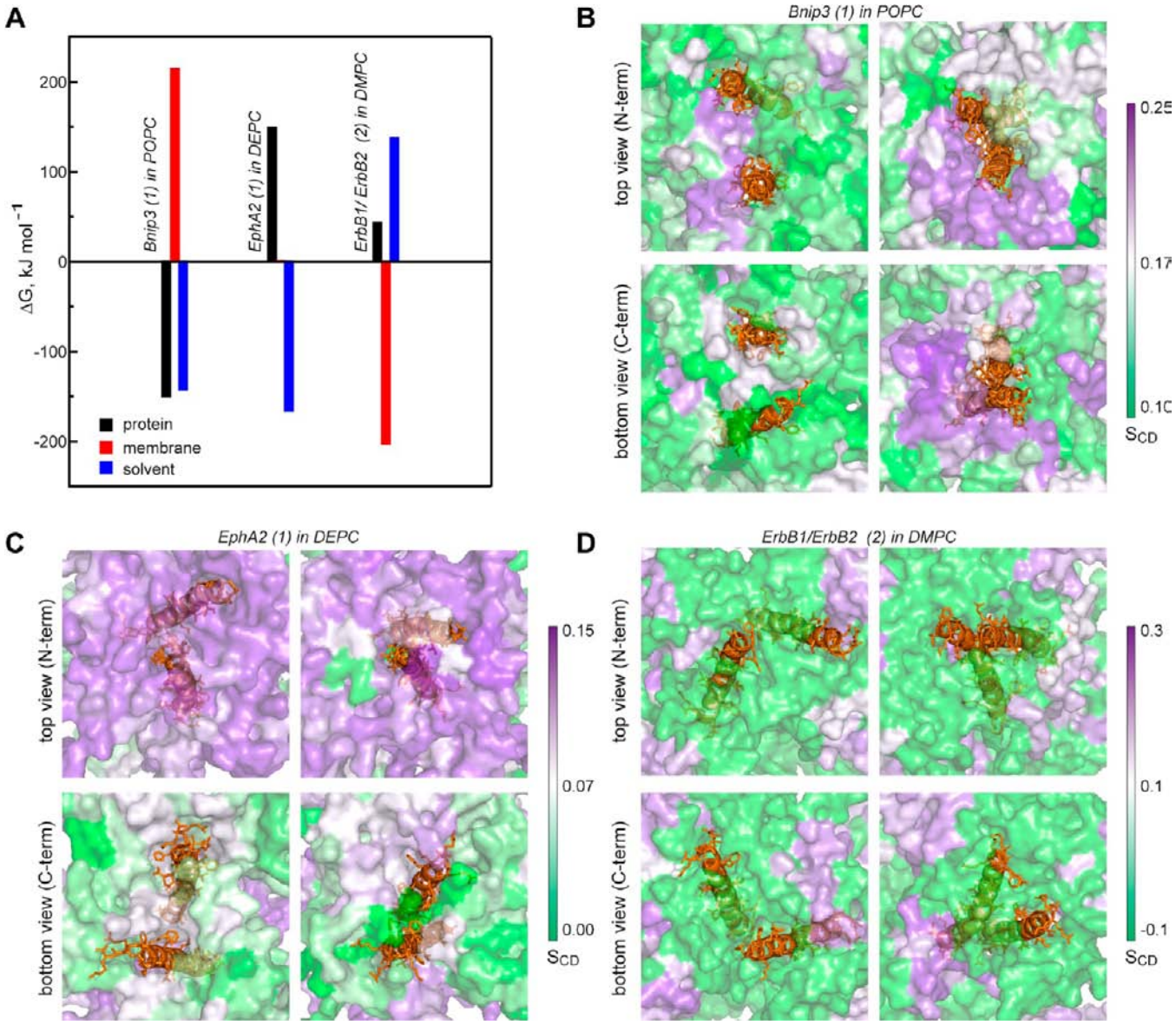

Figure 4. Contribution of membrane to the formation of TM dimers. (A) Examples of free energy decomposition diagrams given for prominently unfavorable (Bnip3 model 1 in POPC), negligible (EphA2 model 2 in DEPC), and strongly favorable (ErbB1/ErbB2 model 2 in DMPC) membrane contributions. (B, C, D) Mapping of lipid order parameters (S_{CD}) on the solvent accessible surface of the bilayer for dimer/bilayer combinations given in the same order as in panel A. Snapshots of fully separated helices and those at a distance corresponding to the free energy minimum are shown independently for both bilayer leaflets. Lipid surfaces are colored according to the scales given on the right sides of panels B–D. Peptides are shown in cartoon-and-sticks representation and colored in orange.

stronger in DPPC lipids than in shorter DLPC or longer DOPC.[47]

In our simulations, model bilayers represent membranes of different types: fluid and relatively amorphous DMPC with thickness of approximately 32 Å measured as the average distance between phosphorus atoms in opposite monolayers of "pure" MD equilibrated membrane ($D_{P\text{-}P}$), moderately thick POPC ($D_{P\text{-}P}$ is approximately 38 Å) with a well-defined water–lipid interface, and prominently thick and fluid DEPC ($D_{P\text{-}P}$ is approximately 42 Å). We have found that the stability of various conformations of dimers depends on the membrane composition. Thus, NMR-like model 1 of Bnip3 exhibits the most negative ΔG value (−74 kJ mol^{-1}) compared with models 2 and 3 in DMPC membrane, retains its stability in POPC, and loses 40% of the dimerization efficiency in DEPC. In contrast, the mirror-like analogue of Bnip3—conformation 3 (similar His-Ser interface, but positive angles χ varying in MD between 40 and 50°)—has anomalously low free energy of association in POPC membrane (−95 kJ mol^{-1}) and undergoes strong dimerization in DEPC membrane. For NMR-like conformation of Bnip3, we have observed a gradual decrease of its similarity to the experimental model[29] upon changing the lipid environment: backbone rmsd's for the structures relaxed in DMPC, POPC, and DEPC membrane are 0.9, 1.2, and 1.7 Å, respectively (Table S1, Supporting Information). Although in the amorphous environment NMR conformation of Bnip3 is the preferential one, decreasing the bilayer flexibility and increasing its thickness may induce a conformational transition to the alternative left-handed structure.

EphA2 exhibits an even more interesting behavior. Previously, a possible switch between the left-handed (NMR-like, model 1) and the right-handed (similar to NMR-structure

dx.doi.org/10.1021/ja303483k | J. Am. Chem. Soc. 2012, 134, 14390–14400

of EphA1, model 2) conformation was hypothesized.[8] According to the values of the free energy of association (Figure 3A), both conformations are almost equally possible in an amorphous DMPC bilayer (ΔG values are −45 and −41 kJ mol^{-1}, respectively). Switching of the environment to POPC makes the right-handed models the most favorable ones (−53 kJ mol^{-1}). In a DEPC bilayer, both left-handed conformations (models 3 and 1, −28, and −27 kJ mol^{-1}, respectively) become more stable as compared to the right-handed one (−22 kJ mol^{-1}). Also, in this membrane relaxed NMR-like EphA2 conformation displays the lowest rmsd from the experimental structure.[8] Thus, preferential formation of the right-handed dimer of EphA2 seems to be possible only in a particular environment similar in its properties to the POPC bilayer.

Finally, for the longest ErbB1/ErbB2 dimer having a relatively weak strength of helix association in the series of studied peptides, the most efficient dimerization is observed for the NMR-like model in a POPC bilayer (1, −45 kJ mol^{-1}). However, this structure deviates considerably from the experimental one[31] exhibiting an rmsd of 2.9 Å. Even in the thick DEPC membrane the conformation closest to the NMR model displays an rmsd of 2.8 Å (model 1), while the most stable one (model 3, −31 kJ mol^{-1}) deviates by up to 3.4 Å from the experimental structure. Interestingly, each simulated membrane "selects" its own favorable conformation of ErbB1/ErbB2 heterodimer—models 2, 1, and 3 in DMPC, POPC, and DEPC, respectively, due to the existence of many equally well-packed and similar conformations of the dimer (see above). Such a structural organization probably allows for a better adaptation of the dimer to the particular lipid surroundings.

What properties of a dimer drive the dimerization in different membrane environments? We found that this effect is specific rather than being shared between different lipid systems. For instance, the scoring function used for ranking dimer structures built from ideal helices (F_{SCOR}) works well in the "simple" DMPC bilayer, where better conformations (according to F_{SCOR} values) also demonstrate higher stability (Figure 3A, Supporting Information, Figure S3). At the same time, POPC and DEPC membranes "select" alternative conformations evaluating dimers in a different way. Thus, POPC favors more compact (smaller SASA) and shorter (smaller L) over more extended and longer dimer configurations (Figure 3 panels B and C). This corresponds well to the hydrophobic match/mismatch concept.[48,49] However, we should mention that simple adaptation of the dimer to the hydrophobic thickness of the membrane can be reflected just in the tilt of the entire complex without conformational transitions, as it has been recently shown for PDGFR-β.[35] Furthermore, among the bilayers under study, POPC displays the best filtering of dimer conformations in terms of differences in their ΔG values. In contrast, in our simulations DEPC possesses the minimal ability of distinguishing between the conformations. This, in turn, makes possible the appearance of more "extreme" or "outlier" structures.

A Particular Role of the Membrane. As it has been seen before, efficiency of helices association as well as the structural properties of dimers are modulated by the lipid environment. To understand better these effects, we have performed free energy decomposition, taking into account individual contributions of a protein, a bilayer, and a solvent (water + ions) to free energy profiles (see Methods). Again, we have observed very distinct pictures for the peptides under study. Thus, the association of Bnip3 is usually accompanied with strong favorable and strong unfavorable contributions from the protein and the membrane, respectively (Supporting Information, Figure S2, Figure 4A). In contrast, regardless of the bilayer type, ErbB1/ErbB2 almost always demonstrates the opposite tendency (Figure S2, Figure 4A), suggesting the membrane-driven dimerization of these peptides. Similarly, EphA2 association is mostly accompanied by unfavorable protein contribution with moderate favorable impact of the membrane (Figure S2). In general, this picture corresponds to the gradation of the dimers established above: strong Bnip3 with the narrow conformational space (Figure 2D), moderate EphA2, and the relatively weak ErbB1/ErbB2 (see above). However, despite the mentioned tendencies, for each dimer we were able to find several types of association scenarios depending on its resulting conformation (predicted model) and the lipid type. Illustrative examples are shown in Figure 4A. Here, one can see that the estimated free energy gains (Figure 3A) can be obtained by various contributions of the main factors. Particularly, the membrane impact can be strongly unfavorable (Bnip3 model 1 in POPC), negligible (EphA2 model 1 in DEPC), and strongly favorable (ErbB1/ErbB2 model 2 in DMPC). We speculate that the origin of such different membrane behavior might depend on the character of the perturbation induced by the presence of a protein in the membrane interior. To illustrate this idea, we have calculated lipid order parameter (S_{CD}) per each molecule along the reaction coordinate used to generate PMF profiles (see Methods). For each sample trajectory with a given helix–helix distance, we have visualized average lipid S_{CD} on the respective solvent accessible surface of the bilayer. Thus, dimerization of Bnip3 helices leads to prominent ordering of lipids in both POPC bilayer leaflets (Figure 4B), which is also associated with unfavorable membrane contribution to the free energy. Although EphA2 perturbs upper (N-terminal) and lower (C-terminal) bilayer leaflets in a different way, its dimerization does not induce prominent ordering or disordering of DEPC lipids, but rather slightly affects their packing (Figure 4C). This is reflected in almost zero impact of the DEPC bilayer on dimerization (Figure 4A). Finally, dimerization of ErbB1 and ErbB2 helices is accompanied with a minor decrease of S_{CD} in both DMPC leaflets (Figure 4D) together with a decrease of the membrane-related part of PMF (Figure 4A). The latter observations support the idea that the efficiency of TM helices dimerization is strongly dependent on the interplay between their primary structures and the membrane composition. Character of the membrane perturbation induced by peptides in monomeric and dimeric states seems to be reflected in the particular membrane contribution to the free energy gain. In our examples, lipid ordering upon dimerization is associated with a prominent increase of membrane influence on PMF (Figure 4A,B), suggesting the possible entropic nature of membrane driving helices association.[50] However, these results are still rather illustrative than representing systematic considerations of the molecular origin of the dimerization driving force. For instance, solvent (water) is another important player: as seen in Figure 4A, it can strongly facilitate or obstruct the association. One of possible reasons here can be that the dimerization also affects premembrane water layers directly by juxtamembrane fragments or through perturbation of the lipid–water interface. However, molecular details of solvent contribution still need to be clarified. This work is in progress now in our lab.

Approximation of Dimer Stability by the Scoring Function. Although free energy calculations in explicit membranes provide the most adequate estimation of dimer stability, they are still computationally demanding when applied to a large number of dimer conformations. Therefore, we have attempted to find a quantitative correlation between the ranking provided by the scoring function and the dimer stability observed in the "simplest" DMPC membrane. Since absolute F_{SCOR} values cannot be directly applied to compare the packing properties of dimers formed by different peptides (e.g., Bnip3, EphA2, and ErbB1/ErbB2), we have centered and normalized them (F^{C}_{SCOR}, see Methods) in order to plot the values calculated in DMPC bilayers against ΔG^{C} and rescaled in the same way (Supporting Information, Figure S3, see above). As seen from the figure, ΔG^{C} is linearly proportional to F^{C}_{SCOR}. The coefficient of proportionality is equal to −0.8. Particularly, the observed correlation means that at least in 64% of cases the best dimer is also the most stable one in DMPC-like membrane. Interestingly, the scoring function does not exhibit significant correlation with any individual energetic contributions of a protein, a membrane, and solvent, neither in DMPC nor in other membranes under study (data not shown), attesting to its general character. According to the data reported in Table 1, for 75% of the peptides (not counting ErbB3, where no NMR-like conformation has been predicted) the structure with the highest F_{SCOR} value is also similar to that obtained from NMR data in micelles or bicelles. Note, that both these mimics represent the less constrained environment as compared to lipid bilayers or cell membranes[22] and result in almost "ideal" conformation of the dimer.

Dimerization Efficiency of TM Domains of RTKs from ErbB Family. Finally, we have estimated the packing score for homo- and heterodimers of TM domains of ErbB receptors (wild-type ErbB1−4 and ErbB2*neu** carrying the mutation V664Q). Since their TM sequences are relatively similar, we normalized the packing efficiency (F^{C}_{SCOR}) across the whole set of the 33 predicted structures (see Methods). We chose all dimers with a maximum normalized packing efficiency above the average and plotted the normalized packing efficiency of their three top-scoring conformations as a function of the dimer crossing angle (Figure 5). It can be seen that heterodimers of ErbB1, ErbB2, and ErbB3, and homodimer of ErbB2*neu** are predicted to be packed most efficiently. The right-handed, NMR-like conformation of ErbB1/ErbB2, its left-handed mirror image and the left-handed ErbB2*neu** homodimer constitute the three dimers that are predicted to associate most strongly. Interestingly, the ErbB2*neu** mutant is known to be involved in oncogenesis.[11] It was proposed that this mutation might block the conformational transition of the receptor to the inactive state.[51] We have found that the two highest-scoring conformations of the ErbB2*neu** homodimer have positive dimer crossing angles, while the wild-type peptide forms both, left-handed (model 1) and right handed, NMR-like (model 2) homodimers. The left-handed dimer was also obtained in a previous modeling study and attributed to the active state of the receptor.[52] In summary, we have found that the V664Q mutation of ErbB2*neu** increases the dimer packing efficiency relative to the wild type and favors the left-handed over the right-handed dimer conformations which is not the case for the wild-type peptide. Importantly, not only the mutant form of ErbB2, but also its heterodimers with ErbB1 and ErbB3 contribute to oncogenesis, for example, in breast cancer.[53,54] This finding supports the high stability predicted for these

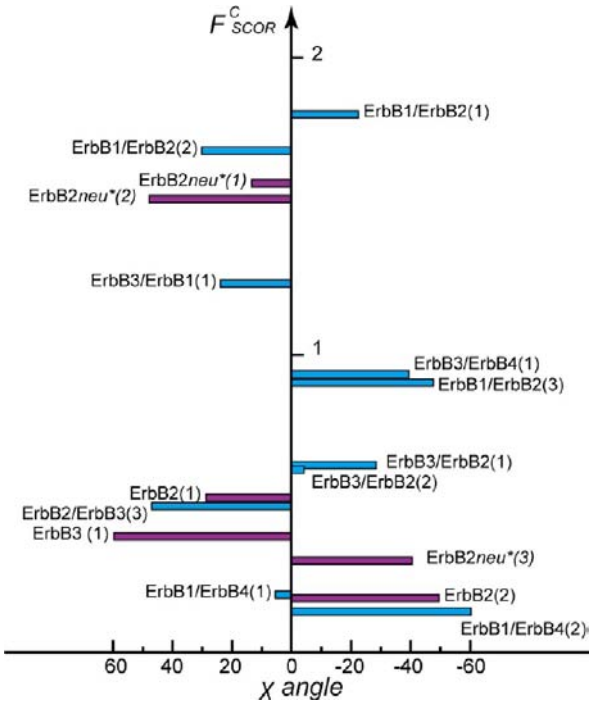

Figure 5. Normalized packing score (F^{C}_{SCOR}) of homo- (violet bars) and heterodimers (blue bars) of TM peptides from the ErbB family plotted as functions of the dimer crossing angle (χ). Only structures with a packing efficiency above the average are indicated (complete set of data is available from Supporting Information, Table S3). For each dimer, three top-scoring conformations (numbered "1″, "2″, and "3") are shown.

dimers by our packing score. Thus we propose that the stability of the ErbB TM domain dimers can be related to the activation strength of the respective full-length complexes. Altogether, dimerization efficiency in ErbB family may be depicted as follows: ErbB1/ErbB2 > ErbB2*neu** > ErbB1/ErbB3 > ErbB3/ErbB4 > ErbB2/ErbB3∼ErbB2 > ErbB3 >ErbB1/ErbB4 > ErbB2/ErbB4 > ErbB1 > ErbB4 (Figure 5, see also Supporting Information, Table S3 for full details). This corresponds well to the fact that ErbB3 tends to form heterodimers, rather than homodimers.[55] Also, such estimations display a good agreement with the results of free energy measurements using FRET techniques in LDAO detergents: ErbB1/ErbB2 > ErbB2/ErbB3 > ErbB1/ErbB3 > ErbB2 > ErbB1 > ErbB2/ErbB4 > ErbB1/ErbB4 > ErbB3 > ErbB3/ErbB4 > ErbB4.[21] Except for some discrepancies, both analyses give similar arrangements of the dimers. Interestingly, the results obtained within our approximation coincide with the dimer stability in a relatively amorphous DMPC membrane. At the same time, the predicted homodimer stability displays almost a reverse correspondence with genetic TOXCAT analysis[20] and respective coarse-grained simulations in a DPPC membrane.[56] A possible explanation of such inconsistency might be related to the crucial role of a particular membrane environment, which varies in all mentioned cases. For instance, a bacterial membrane (the host environment in TOXCAT experiments) promotes destabilization of a dimer as compared to its association in detergents and model bilayers.[15] Also, the coarse-grained membrane may not be detailed enough to distinguish between such very similar dimers. Finally, the role of juxtamembrane regions contributing to stabilization of TM dimers[19,15] is not

dx.doi.org/10.1021/ja303483k | J. Am. Chem. Soc. 2012, 134, 14390−14400

considered equally in the aforementioned studies and is almost ignored in our estimations.

CONCLUSION

In the present study, we have shown that our surface-based PREDDIMER approach is able to predict the conformations of TM dimers in good agreement with the experiment. Our approach also provides a powerful tool for the exploration of conformational heterogeneity in TM helix−helix dimers as well as for simple estimation of the strength of their self-association. Although for each of the considered 18 homo- and heterodimers the prediction has been based on the same principles, particular contributions of landscape complementarity and hydrophobic matching at the protein−protein and protein−lipid interface exhibit sequence-dependent character and cannot be equally extrapolated to any TM fragments. A balance between all factors (e.g., ErbB2 dimer) can be contrasted with the predominance of geometrical factors (e.g., ErbB1/ErbB2), hydrophobic properties of the interhelical region (e.g., GpA), or properties of the dimer surface exposed to lipids (e.g., PDGFR-β). Moreover, the observed dimeric structure can be strongly modulated by the lipid surrounding. Using microsecond all-atom MD simulations of the predicted dimers in different model membranes, we have found that specific lipid bilayers preferentially stabilize certain dimer conformations, demonstrating in this way structural tuning of the dimer in response to membrane characteristics. This suggests a multistate organization of TM helical dimers in heterogeneous membranes, and emphasizes the importance of considering their conformational variability in designing potent selective modulators of dimerization acting on pharmaceutically relevant targets in the natural milieu of cell membranes. Finally, decomposition of the integral PMF profiles into individual terms emphasizes that the observed free energy gain upon dimerization can be obtained by various contributions of the main factors involved—proteins, membrane, and solvent. We have found that the character of membrane perturbation induced by transition of TM peptides from monomeric to dimeric states might underline the particular membrane influence on PMF. However, further analysis of the atomistic picture behind the structural adaptation of proteins and membrane in the course of TM helix association and a better understanding of the role of solvent in this process are still required to elucidate the molecular origin of the driving force of dimerization. Currently, this work is being carried out by the authors.

METHODS

Prediction of Packing Properties of TM Helical Dimers. Spatial structures of the dimers formed by TM helical fragments under study were built using PREDDIMER algorithm (Figure 1, see also ref 17). For each sequence, its respective TM helix was constructed in an ideal conformation using the standard statistics of side chain dihedrals. A helical surface with mapped hydrophobic/hydrophilic properties was calculated using PLATINUM software.[57] Hydrophobicity at each surface point was estimated using the molecular hydrophobicity potential (MHP) approach.[28,58] All further steps were performed using the PREDDIMER package (available soon at the laboratory webpage). Upon prediction of the dimer structure, both rotation angles ($\alpha1$, $\alpha2$) around axes of the helices (from 0 to 360°, with 6° step) along with a number of crossing angles (χ) between the axes of the monomers (from −60 to 60, with 5° step) were systematically varied, thus giving in total about 10^5 variants (61 × 61 × 25). Matching between the helical landscapes and spatial distributions of hydrophobic properties for each combination of surface patches interpolated on a regular grid and representing helical surface with respect to rotation and tilt angles were calculated using a scoring function F_{INT} ($\alpha1$, $\alpha2$, χ, R, d), where R is the distance between helical axes and d is the shift along the helical axis. For each angle χ, the spatial structure of a dimer with the best value of F_{INT} ($\alpha1$, $\alpha2$, R, d) was reconstructed and geometrically optimized using a simple energy minimization procedure in vacuum. The packing quality of each dimeric structure was quantified using a scoring function F_{SCOR} (*Pack*, *Int*, *Env*), where *Pack* is the term corresponding to a relative number of atoms packed within a structures, *Int* is the term accounting MHP complementarity on the helical interface, and *Env* is the term estimating correspondence of polar and structural properties of a dimer surface exposed to lipid environment with that observed in a model set of spatial structures of TM domains of different membrane proteins (see Supporting Information for details). All predicted structures were clustered using calculations of root-mean-square deviations (rmsd) and correlations between interhelical contact maps taken over all solutions. Resulting structures were subsequently sorted according to F_{SCOR} values of representative models.

MD Relaxation of Dimer Conformations. All simulations were performed using the GROMACS 4.0.7 package[59] and the GROMOS96 force field (43*a*2*x* parameter set). MD simulations were carried out with a time step of 2 fs, using 3D periodic boundary conditions, in the isothermal−isobaric (NPT) ensemble with a semi-isotropic pressure of 1 bar and a constant temperature of 315 K (to ensure the liquid crystalline phase of the lipid bilayers). The pressure and the temperature were controlled using the Berendsen thermo- and barostat[60] with 1.0 and 0.1 ps relaxation parameters, respectively, and a compressibility of 4.5×10^{-5} bar^{-1} for the barostat. A twin-range (10/12 Å) spherical cutoff function was used to truncate van-der-Waals interactions. Electrostatic interactions were treated using the particle-mesh Ewald summation (real space cutoff 10 Å and 1.2 Å grid with fourth-order spline interpolation).

Dimer conformations obtained using PREDDIMER software were extended by several polar residues at N- and C-termini (see Supporting Information, Table S4) to keep their correct positioning in a membrane and then were inserted in pre-equilibrated DMPC, POPC, or DEPC bilayers of 128 lipids and solvated by SPC water.[61] In the beginning of the simulations, the systems were equilibrated by energy relaxation *via* 5×10^4 steps of steepest descent minimization followed by heating from 5 K to the temperature of simulations (315 K) during 50-ps MD run and 2-ns MD run at 315 K with fixed positions of the peptides' atoms. Such equilibration is necessary for minimization of bilayer distortion induced by insertion of the peptides and removal of several lipid molecules. Then, water molecules located in the bilayer interior were removed, and the long-term (50 ns) collection MD runs were carried out.

Estimation of the Free Energy of Dimer Association in Membranes. To calculate the PMF as a function of helix−helix distance, a total of 66 windows were constructed from r_{HH} = 7 Å to r_{HH} = 20 Å every 0.2 Å, where r_{HH} is the distance between the monomers' backbone centers of mass. An initial structure in each window was generated by 10 ns MD equilibration with positions of the monomers' backbone atoms fitted to the reference structure. The latter one was obtained from the starting model by translation of monomers in the membrane plane along the line, connecting their centers of mass. Each system was then subjected to 1 ns equilibration and 15 ns production MD runs with a helix−helix distance force constant of 10000 kJ mol^{-1} $Å^{-1}$ to restrain r_{HH} near the corresponding target value. After 15 ns production run in each window, the total PMF of a dimer association $W(r_{HH})$, was calculated by integrating the mean force $\langle F(r_{HH})\rangle$ along r_{HH} as described elsewhere.[44,45] To estimate the accuracy of PMF calculation, the MD trace was divided into three 5-ns parts, which were subsequently used in independent calculations of the related profiles. Energy decomposition was performed using the following scheme: (1) reduction of the initial trajectory to one containing only parts of the system (protein; protein+membrane; protein+solvent); (3) recalculation of forces from coordinates in the reduced trajectory; (3) projection of forces, acting on the protein

atoms, to r_{HH} and averaging; (4) PMF calculation (integration); (5) subtraction of PMF for protein (if needed). Input trajectories were collected with a frame separation of 10 ps and that results in different statistics for energy decomposition and calculation of the total PMF. Consequently, this induces an increase of the errors in decomposition, while profile shapes and positions of energy minima remain the same.

Analysis of Dimer Structural Properties. For ideal and MD-relaxed conformations of each dimer, the following characteristics were calculated using utilities specially developed for this purpose: length of TM region (L); crossing angle between helical axes (χ); solvent accessible surface area (SASA); root-mean-square deviation from the experimental structure (rmsd) calculated over the backbone atoms; packing efficiency (F_{SCOR}, see above); free energy of association (ΔG) as an integral calculated over PMF profiles. Visualization of F_{SCOR} and χ distributions along the coordinates ($\alpha 1$, $\alpha 2$) was performed in MATLAB (R2009a). Normalized values of F^{C}_{SCOR} for a set of three top-ranked dimer conformations were calculated as: $F^{C}_{SCOR} = (F_{SCOR} - \langle F_{SCOR}\rangle)/\mathrm{std}.F_{SCOR}$, where $\langle F_{SCOR}\rangle$ and $\mathrm{std}.F_{SCOR}$ are the mean and standard deviation within the set. ΔG^{C} values were calculated using the same formalism. Calculations of F^{C}_{SCOR} values for dimers in the ErbB family were performed using means and standard deviations obtained for the entire set of 33 structures (11 × 3).

Mapping of Lipid Order Parameters on the Membrane Surface. Deuterium lipid order parameter (S_{CD}) per each molecule was calculated along the reaction coordinate used to generate PMF profiles. Each sample trajectory with a given helix−helix distance (see above) was divided into 15 1-ns fragments and used to calculate individual S_{CD} values for each of the lipid molecules in the system with the help of the standard *g_order* tool from the GROMACS 4.0.7 package.[59] Average S_{CD} values obtained in this way were used to color the respective solvent accessible surface of the bilayer.

■ ASSOCIATED CONTENT

Supporting Information

Table with rmsd values between MD and NMR dimeric structures; table with values of crossing angles for MD relaxed dimers; table with ErbBs homo- and heterodimers ranked according to normalized F_{SCOR} values; table with full sequences of peptides used in MD simulations; figure showing PMF profiles for dimers in different membranes; figure showing decomposition of PMF profiles for dimers in different membranes; figure illustrating correlation between the dimer packing efficiency (F_{SCOR}) and the dimer stability in DMPC membrane; PREDDIMER algorithm details. This material is available free of charge via the Internet at http://pubs.acs.org.

■ AUTHOR INFORMATION

Corresponding Author

newant@gmail.com

Notes

The authors declare no competing financial interest.

■ ACKNOWLEDGMENTS

This work was supported by the Ministry of Education and Science of the Russian Federation (MK-8439.2010.4), by the Federal Target Program "Research and development in priority fields of Russian scientific and technological complex in 2007−2013, by the Russian Foundation for Basic Research, and by the RAS Programme "Basic fundamental research for nanotechnologies and nanomaterials". Access to computational facilities of the Joint Supercomputer Center RAS (Moscow) and Moscow Institute of Physics and Technology is gratefully acknowledged.

■ REFERENCES

(1) Bennasroune, A.; Fickova, M.; Gardin, A.; Dirrig-Grosch, S.; Aunis, D.; Cremel, G.; Hubert, P. *Mol. Biol. Cell* **2004**, *15*, 3464.
(2) Bennasroune, A.; Gardin, A.; Auzan, C.; Clauser, E.; Dirrig-Grosch, S.; Meira, M.; Appert-Collin, A.; Aunis, D.; Cremel, G.; Hubert, P. *Cell. Mol. Life Sci.* **2005**, *62*, 2124.
(3) Li, E.; Hristova, K. *Biochemistry* **2006**, *45*, 6241.
(4) Cymer, F.; Schneider, D. *Cell Adh. Migr.* **2010**, *4*, 299.
(5) Cymer, F.; Veerappan, A.; Schneider, D. *Biochim. Biophys. Acta* **2012**, *1818*, 963.
(6) Li, E.; Wimley, W. C.; Hristova, K. *Biochim. Biophys. Acta* **2012**, *1818*, 183.
(7) Fleishman, S. J.; Schlessinger, J.; Ben-Tal, N. *Proc. Natl. Acad. Sci. U.S.A.* **2002**, *99*, 15937.
(8) Bocharov, E. V.; Mayzel, M. L.; Volynsky, P. E.; Mineev, K. S.; Tkach, E. N.; Ermolyuk, Y. S.; Schulga, A. A.; Efremov, R. G.; Arseniev, A. S. *Biophys. J.* **2010**, *98*, 881.
(9) Roskoski, R., Jr. *Biochem. Biophys. Res. Commun.* **2004**, *319*, 1.
(10) Moore, D. T.; Berger, B. W.; DeGrado, W. F. *Structure* **2008**, *16*, 991.
(11) Shahidullah, K.; Krishnakumar, S. S.; London, E. *J. Mol. Biol.* **2010**, *396*, 209.
(12) Engelman, D. M. *Nature* **2005**, *438*, 578.
(13) Simons, K.; Gerl, M. J. *Nat. Rev. Mol. Cell Biol.* **2010**, *11*, 688.
(14) Schafer, L. V.; de Jong, D. H.; Holt, A.; Rzepiela, A. J.; de Vries, A. H.; Poolman, B.; Killian, J. A.; Marrink, S. J. *Proc. Natl. Acad. Sci. U S A* **2011**, *108*, 1343.
(15) Hong, H.; Bowie, J. U. *J. Am. Chem. Soc.* **2011**, *133*, 11389.
(16) Bocharov, E. V.; Volynsky, P. E.; Pavlov, K. V.; Efremov, R. G.; Arseniev, A. S. *Cell Adh. Migr.* **2010**, *4*, 284.
(17) Polyansky, A. A.; Volynsky, P. E.; Efremov, R. G. *Adv. Protein Chem. Struct. Biol.* **2011**, *83*, 129.
(18) Yin, H.; Slusky, J. S.; Berger, B. W.; Walters, R. S.; Vilaire, G.; Litvinov, R. I.; Lear, J. D.; Caputo, G. A.; Bennett, J. S.; DeGrado, W. F. *Science* **2007**, *315*, 1817.
(19) Oates, J.; King, G.; Dixon, A. M. *Biochim. Biophys. Acta* **2010**, *1798*, 605.
(20) Mendrola, J. M.; Berger, M. B.; King, M. C.; Lemmon, M. A. *J. Biol. Chem.* **2002**, *277*, 4704.
(21) Duneau, J. P.; Vegh, A. P.; Sturgis, J. N. *Biochemistry* **2007**, *46*, 2010.
(22) Hong, H.; Blois, T. M.; Cao, Z.; Bowie, J. U. *Proc. Natl. Acad. Sci. U.S.A.* **2010**, *107*, 19802.
(23) McDonnell, A. V.; Jiang, T.; Keating, A. E.; Berger, B. *Bioinformatics* **2006**, *22*, 356.
(24) Apgar, J. R.; Gutwin, K. N.; Keating, A. E. *Proteins* **2008**, *72*, 1048.
(25) Langosch, D.; Heringa, J. *Proteins* **1998**, *31*, 150.
(26) Bowie, J. U. *Curr. Opin. Struct. Biol.* **2011**, *21*, 42.
(27) Kordyukova, L. V.; Serebryakova, M. V.; Polyansky, A. A.; Kropotkina, E. A.; Alexeevski, A. V.; Veit, M.; Efremov, R. G.; Filippova, I. Y.; Baratova, L. A. *Biochim. Biophys. Acta* **2011**, *1808*, 1843.
(28) Efremov, R. G.; Chugunov, A. O.; Pyrkov, T. V.; Priestle, J. P.; Arseniev, A. S.; Jacoby, E. *Curr. Med. Chem.* **2007**, *14*, 393.
(29) Bocharov, E. V.; Pustovalova, Y. E.; Pavlov, K. V.; Volynsky, P. E.; Goncharuk, M. V.; Ermolyuk, Y. S.; Karpunin, D. V.; Schulga, A. A.; Kirpichnikov, M. P.; Efremov, R. G.; Maslennikov, I. V.; Arseniev, A. S. *J. Biol. Chem.* **2007**, *282*, 16256.
(30) Bocharov, E. V.; Mayzel, M. L.; Volynsky, P. E.; Goncharuk, M. V.; Ermolyuk, Y. S.; Schulga, A. A.; Artemenko, E. O.; Efremov, R. G.; Arseniev, A. S. *J. Biol. Chem.* **2008**, *283*, 29385.
(31) Mineev, K. S.; Bocharov, E. V.; Pustovalova, Y. E.; Bocharova, O. V.; Chupin, V. V.; Arseniev, A. S. *J. Mol. Biol.* **2010**, *400*, 231.
(32) Bocharov, E. V.; Mineev, K. S.; Volynsky, P. E.; Ermolyuk, Y. S.; Tkach, E. N.; Sobol, A. G.; Chupin, V. V.; Kirpichnikov, M. P.; Efremov, R. G.; Arseniev, A. S. *J. Biol. Chem.* **2008**, *283*, 6950.

(33) Mineev, K. S.; Khabibullina, N. F.; Lyukmanova, E. N.; Dolgikh, D. A.; Kirpichnikov, M. P.; Arseniev, A. S. *Biochim. Biophys. Acta* **2011**, *1808*, 2081.
(34) MacKenzie, K. R.; Prestegard, J. H.; Engelman, D. M. *Science* **1997**, *276*, 131.
(35) Muhle-Goll, C.; Hoffmann, S.; Afonin, S.; Grage, S. L.; Polyansky, A. A.; Windisch, D.; Zeitler, M.; Buerck, J.; Ulrich, A. S. *J. Biol. Chem.* **2012**, *287*, 26178.
(36) Vereshaga, Y. A.; Volynsky, P. E.; Pustovalova, J. E.; Nolde, D. E.; Arseniev, A. S.; Efremov, R. G. *Proteins* **2007**, *69*, 309.
(37) Bu, L.; Im, W.; Brooks, C. L., 3rd *Biophys. J.* **2007**, *92*, 854.
(38) Gervais, C.; Wust, T.; Landau, D. P.; Xu, Y. *J. Chem. Phys.* **2009**, 130.
(39) Zhang, J.; Lazaridis, T. *Biophys. J.* **2009**, *96*, 4418.
(40) Fleishman, S. J.; Ben-Tal, N. *J. Mol. Biol.* **2002**, *321*, 363.
(41) Park, Y.; Elsner, M.; Staritzbichler, R.; Helms, V. *Proteins* **2004**, *57*, 577.
(42) Samna Soumana, O.; Garnier, N.; Genest, M. *Eur. Biophys. J.* **2007**, *36*, 1071.
(43) Lemmon, M. A.; Flanagan, J. M.; Treutlein, H. R.; Zhang, J.; Engelman, D. M. *Biochemistry* **1992**, *31*, 12719.
(44) Henin, J.; Pohorille, A.; Chipot, C. *J. Am. Chem. Soc.* **2005**, *127*, 8478.
(45) Lee, J.; Im, W. *J. Am. Chem. Soc.* **2008**, *130*, 6456.
(46) Lawrie, C. M.; Sulistijo, E. S.; MacKenzie, K. R. *J. Mol. Biol.* **2010**, *396*, 924.
(47) Janosi, L.; Prakash, A.; Doxastakis, M. *Biophys. J.* **2010**, *99*, 284.
(48) Sparr, E.; Ash, W. L.; Nazarov, P. V.; Rijkers, D. T.; Hemminga, M. A.; Tieleman, D. P.; Killian, J. A. *J. Mol. Biol.* **2005**, *280*, 39324.
(49) Holt, A.; Killian, J. A. *Eur. Biophys. J.* **2010**, *39*, 609.
(50) Bocharov, E. V.; Mineev, K. S.; Goncharuk, M. V.; Arseniev, A. S. *Biochim. Biophys. Acta* **2012**, *1818*, 2158.
(51) Beevers, A. J.; Damianoglou, A.; Oates, J.; Rodger, A.; Dixon, A. M. *Biochemistry* **2010**, *49*, 2811.
(52) Prakash, A.; Janosi, L.; Doxastakis, M. *Biophys. J.* **2011**, *101*, 1949.
(53) Lee-Hoeflich, S. T.; Crocker, L.; Yao, E.; Pham, T.; Munroe, X.; Hoeflich, K. P.; Sliwkowski, M. X.; Stern, H. M. *Cancer Res.* **2008**, *68*, 5878.
(54) Gollamudi, M.; Nethery, D.; Liu, J.; Kern, J. A. *Lung Cancer* **2004**, *43*, 135.
(55) Tao, R. H.; Maruyama, I. N. *J. Cell Sci.* **2008**, *121*, 3207.
(56) Prakash, A.; Janosi, L.; Doxastakis, M. *Biophys. J.* **2010**, *99*, 3657.
(57) Pyrkov, T. V.; Chugunov, A. O.; Krylov, N. A.; Nolde, D. E.; Efremov, R. G. *Bioinformatics* **2009**, *25*, 1201.
(58) Efremov, R. G.; Gulyaev, D. I.; Vergoten, G.; Modyanov, N. N. *J. Protein Chem.* **1992**, *11*, 665.
(59) Hess, B.; Kutzner, C.; van der Spoel, D.; Lindahl, E. *J. Chem. Theory Comput.* **2008**, *4*, 435.
(60) Berendsen, H. J. C.; Postma, J. P. M.; van Gunsteren, W. F.; DiNola, A.; Haak, J. R. *J. Chem. Phys.* **1984**, *81*, 3684.
(61) Berendsen, H. J. C.; Postma, J. P. M.; van Gunsteren, W. F.; Hermans, J. *Interaction Models for Water in Relation to Protein Hydration*: Reidel: Dordrecht, The Netherlands, 1981.